Exploring the Binding Site of C-Terminal Hsp90 Inhibitors

Miriam Sgobba, Rosetta Forestiero, Gianluca Degliesposti, and Giulio Rastelli*

Dipartimento di Scienze Farmaceutiche, Università di Modena e Reggio Emilia, via Campi 183, 41125 Modena, Italy

Received May 10, 2010

Abstract: The 90 kDa heat shock protein (Hsp90) is a prominent target for anticancer drug discovery. While its N-terminal domain has been widely exploited, several lines of evidence are emerging in favor of targeting its C-terminal domain to conceive innovative drugs based on perturbation of the dimer interface. Here, we describe the application of several computational approaches useful to predict the location of the C-terminal binding site.

In pathological conditions the 90 kDa heat shock protein (Hsp90) is responsible for the refolding and stabilization of a number of damaged proteins involved in the uncontrolled proliferation and differentiation of cells.[1,2] The interactions with these important regulatory proteins and the role of Hsp90 in activating their related mutant forms make Hsp90 an attractive and interesting pharmacological target in antitumor therapies. Indeed, the inhibition of Hsp90 induces cellular apoptosis and the disruption of multiple signaling pathways important for the growth and viability of cancer cells. Based on this evidence, interest in discovering new compounds able to inhibit Hsp90 has grown considerably. To date, while several inhibitors are known to bind at the N-terminal (NT) domain and compete with the adenosine 5′-triphosphate (ATP) substrate, it is assumed that an additional binding site is found in the C-terminal (CT) domain, i.e., the domain responsible for the dimerization of Hsp90.[3−5] Compounds targeting the CT domain have a completely different mechanism of action, as they inhibit Hsp90 by disrupting or preventing the formation of the dimer essential for chaperone function and interfere with Hsp90−client proteins interactions.[6,7] In view of these findings, there is general excitement about this new interesting possibility of inhibiting Hsp90, as testified by the increasing number of CT inhibitors disclosed so far, such as novobiocin (NB) and coumermycin A1, A4, and DHN2 and many others based on the coumarin scaffold.[8−11] However, the concept that Hsp90 can be inhibited by interfering with the CT domain still needs to be proved on structural grounds, because crystal structures of Hsp90/CT inhibitors have not been reported so far. Consequently, the CT domain is still unexplored for structure-based drug design, and the absence of structural information is making the design of new CT Hsp90 inhibitors very challenging.

In the present work, the CT binding site has been investigated with several computational approaches, and possible binding modes of selected inhibitors have been proposed in order to pave the way for the rational design and identification of next-generation CT inhibitors. Starting from a homology model of full-length human Hsp90 (hHsp90), we have generated an ensemble of protein conformations using molecular dynamics (MD) simulations. By exploiting time-dependent structural features of Hsp90, binding site predictions and docking simulations were able to sample preferential ligand binding sites and binding modes in a multiconformational ensemble of states of the protein. This type of approach has proven successful in drug discovery investigations where advantages of docking algorithms were combined with dynamic structural information of the target protein to explicitly account for the flexibility of both ligand and receptor.[12,13]

To date a crystal structure of human Hsp90 containing the CT domain is not available, therefore its three-dimensional structure was obtained using homology modeling techniques [see Supporting Information (SI) for details].

Since Hsp90 is an ATP-dependent protein and the hydrolysis of the nucleotide triggers drastic conformational changes assumed to be responsible for the folding and release of client proteins, different conformational states of Hsp90 were examined. These mainly involve two predominant conformations coexisting in equilibrium, an open apo conformation and a closed, tense state of the chaperone when bound to ATP.[14−16] The three-dimensional structures of these two conformational states were solved by X-ray crystallography for full-length *Escherichia coli* HtpG and yeast Hsp90 (PDB codes 2IOQ and 2CG9, respectively).[15,17] Since biochemical data have shown that the CT binding site is accessible only when the NT domain is occupied,[3] the X-ray structure of yeast full-length Hsp90 (61% identical to hHsp90) cocrystallized with adenylyl imidodiphosphate (AMPPNP) at the NT (PDB code 2CG9) was considered the most biologically relevant conformation of the chaperone useful as template for the construction of the full-length human Hsp90 homology model. In addition to this, homology model representatives of the open, apo state were built based on the structure of *E.coli* HtpG to compare the results obtained with the closed state. Among 100 homology models of the closed state of hHsp90 thus produced, the best was selected for further structural refinement with molecular mechanics in water. This model showed a good superimposition with the template [root-mean-squared deviation (rmsd) value of Cα atoms is 0.9 Å, see Figure 1 in Supporting Information) and proved satisfactory for Prosa, DOPE, and PROCHECK,[18−20] (with scores of −14.74, −142 546, and −0.34, respectively), suggesting that the model was a good starting point for the subsequent generation of protein conformations with MD. The solvated structure was subjected to 10 ns MD simulations in a physiological environment, and an ensemble of 500 conformations was extracted for subsequent analysis (see Supporting Information for details). During MD, the NT domain remained relatively fixed to the middle (M) domain like a "rigid body", while a bent movement of NT/M domains over the CT, allowed by a long flexible tether

* Corresponding author. E-mail: giulio.rastelli@unimore.it. Telephone: (0039) 059-2055145.

10.1021/ci1001857 © 2010 American Chemical Society
Published on Web 09/09/2010

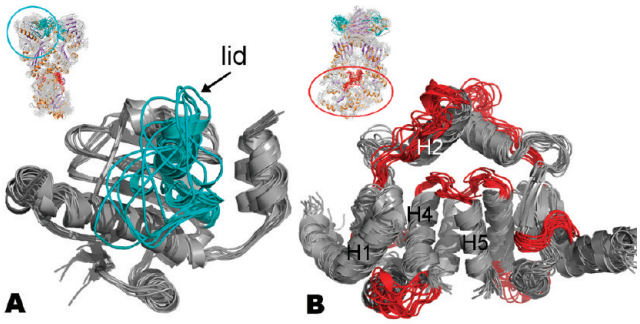

Figure 1. Motions of the ATP lid (cyan, A) and several segments within the CT domain (red, B) during MD of human Hsp90.

that links M and CT, was observed. Such motions are in agreement with electron microscopy and small-angle X-ray scattering studies and several X-ray structures of yeast and *E.coli* Hsp90 in different conformations.[15,21−23] Focusing attention on each domain, our simulations showed that several segments of the protein are considerably flexible. One of these corresponds to the "lid" segment located onto the NT ATP binding site (cyan, Figure 1A), which was shown to flip ∼180° during the ATPase cycle of the chaperone in several X-ray crystal structures. In the CT domain, a loop belonging to the region of helix H2 proved highly flexible (Figure 1B). This observation is consistent with the fact that this segment is disordered in yeast and *E.coli* full-length Hsp90 crystal structures (PDBcodes 2CG9 and 2IOQ). In addition to this region, other segments of the CT domain are flexible (red, Figure 1B). Notably, using the refined homology model of the protein as reference structure, the average rmsd value calculated over all atoms belonging to CT plus a portion of the middle domain (sM) next to it (the so-called sM-CT construct) was 4.65 ± 0.25 Å. Such a high value suggests that the CT and its adjoining domain explore large structural fluctuations during MD, which in turn may affect the shape, volume, and exposure of the potential binding cavities under investigation, supporting the rationale of our multiconformational approach for binding site identification and ligand binding modes assessment.

The binding site identification step was carried out on the 500 Hsp90 conformations with three independent binding site search methods based on different levels of theory. The first two, AutoLigand and SiteMap, exploit the protein structure alone to predict a binding site,[24,25] while the third, AutoDock, with blind docking settings, performs docking simulations on large surfaces of the protein to get unbiased mapping of ligands and to obtain more detailed information about ligand−protein interactions.[26−28] Consensus results were used to identify the most interesting pockets to perform the subsequent extensive docking simulations of known CT inhibitors and to finally select the most likely CT binding site.

AutoLigand and SiteMap identify ligand binding sites by filling protein cavities with points (see Supporting Information for details). By selecting all residues around 2 Å from these points and by computing their occurrence frequency along the conformational ensemble of Hsp90, consensus sites could be extracted. Figure 2 (see also Figure 2 in Supporting Information) shows pockets identified by both methods. As can be observed, AutoLigand and SiteMap gave similar results by detecting residues lining the boundary of

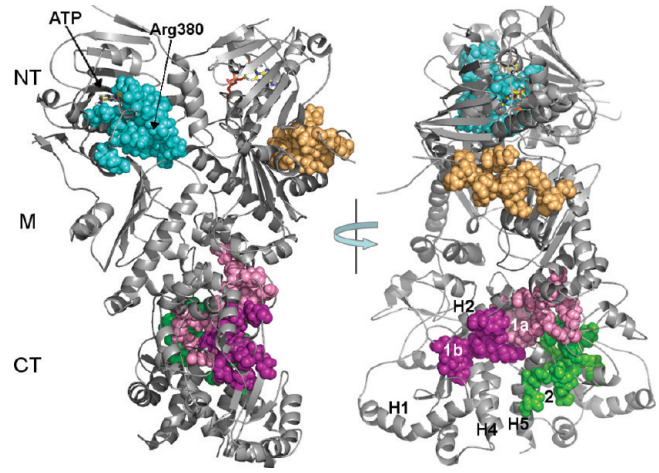

Figure 2. Binding site identification obtained with AutoLigand among all Hsp90 conformations sampled during MD. The known NT-ATP binding site was clearly detected (cyan). Three cavities were identified in CT domain, pck1a (pink), pck1b (violet), and pck2 (green).

similar pockets. Within the NT domain, which can be used to test the protocol, predicted residues belonged to the known ATP binding site and included key residues Asp93, Asn51, Gly137, Phe138, and Arg380 plus aminoacids in the lid segment. Notably, these results fully agree with the considerable structural information available from the X-ray structures of Hsp90 with ATP and NT inhibitors, thus validating the usefulness and accuracy of these methods in detecting ligand binding cavities. Furthermore, although the lid segment was highly flexible during MD and changed the opening and volume of the NT pocket, predicted residues belonging to this segment were correctly recognized as the boundary of the binding site in the vast majority of the conformations accessible to Hsp90 during MD. This indicates that the multiconformation approach correctly pointed toward the involvement of these residues in ligand binding. In the M domain, while SiteMap did not recognize a specific pocket identifying residues spread on the length of the domain, AutoLigand detected a cavity between the NT and M domains located next to the charged linker region (Lys204−Leu220 and Gln287−Pro295). Since this region was truncated in our model given that the corresponding linker was disordered in the template X-ray structure, this pocket could be an artifact arising from the use of an incomplete structure. Nonetheless, the possibility of an additional pocket between NT and M domains cannot be ruled out and needs further investigation. A binding site in this region, if present, would be consistent with a recent work that identifies a region between the NT and M domains able to accommodate a new allosteric inhibitor of Hsp90 not related to a coumarin scaffold.[29] Finally, AutoLigand and SiteMap detected additional cavities within the CT domain. One of these (called pck1) corresponds to a pocket previously detected using a truncated model of CT Hsp90 alone in a single structure approach.[30] Analyzing the snapshots extracted from the present MD simulations, the volume of pck1 varied from 817 to 1580 Å^3. This great variability can be attributed: (i) to the presence of the nearby M domain that forces helix H2 to remain closer to the four-helix bundle of the CT domain and (ii) to movements of side chains of residues lining the boundary of pck1. These movements often split the cavity into two subpockets, a central (pck1a) and side

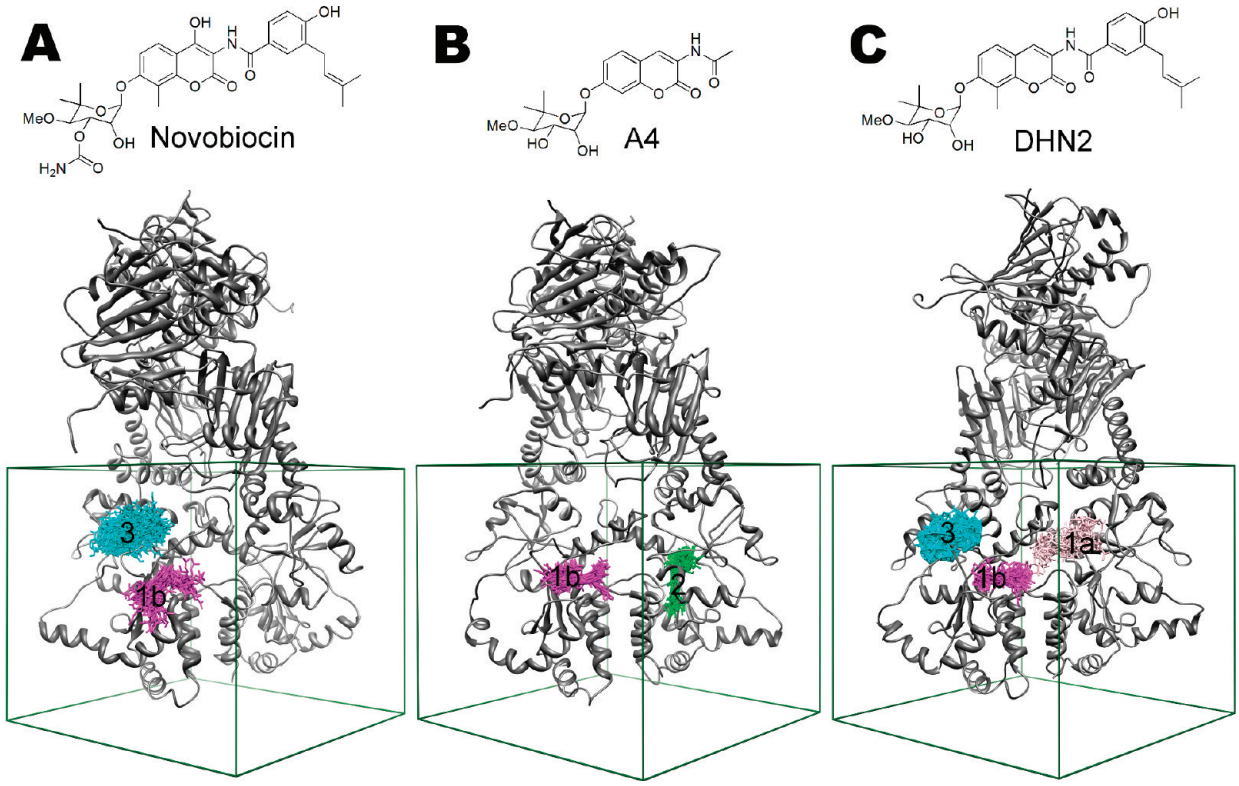

Figure 3. Blind docking results of (A) NB, (B) A4, and (C) DHN2. The ligands docked mainly in four pockets: pck1a (pink), pck1b (violet), pck2 (green), and pck3 (cyan).

(pck1b) one. In particular, we found that the closure and opening of pck1 can be ascribed to a large and time-dependent movement of the side chain of Lys615 in H2, as testified by the fluctuation of the distance between the protonated nitrogen of this lysine and the backbone carbonyl of Glu679 in the H4−H5 loop (see Figure 3 in Supporting Information). Interestingly, when the hydrogen bond is present, pck1 is split into pck1a and pck1b subpockets, while a unique pocket is formed when the hydrogen bond is absent. It is worth noting that this behavior could not be detected in the single truncated CT structure analyzed before, reinforcing the concept that a multiconformational approach on full-length Hsp90 is required. Besides pck1a and pck1b, an additional cavity (pck2) located between helices H4′−H5 and β-sheets was detected (Figure 2). This can be considered as a further hypothetical binding site in CT domain.

Blind docking simulations of three known CT inhibitors, novobiocin (NB), A4, and DHN2 (Figure 3), were performed with AutoDock by scanning the entire sM-CT domain of each structure sampled during MD (see Supporting Information for methodological details). For each protein conformation the lowest-energy ligand pose was retained, resulting in 500 best-score orientations per molecule which were finally ranked and clustered based on AutoDock energy scores and geometrical criteria in order to identify preferential pockets able to accommodate the inhibitors. The results for NB, A4, and DHN2 blind dockings are shown in the histograms of Figure 4 in the Supporting Information, where each bar represents a cluster to which the number of ligand orientations and the lowest-energy score are associated. The location of the most interesting clusters is shown in Figure 3A−C. Two large clusters emerged from the histogram of NB. One of these contains 28 orientations, the best one with a score of −8.56 kcal/mol, and identifies pck1b. Interestingly, the other cluster (59 orientations, −10.47 kcal/mol) covers a region that was not detected by previous methods and interfaces sM and CT domains (called pck3, Figure 3A). An additional cluster, with a best score of −9.06 kcal/mol and containing 22 orientations, is present in the histograms (see Figure 4, Supporting Information). However, its location is again ascribable to previously described pck3, albeit with different ligand poses, and therefore placed in a separate cluster. In the case of A4 blind docking, two large clusters were identified. The most populated of the two (having 57 orientations) identifies pck1b, and the other (43 orientations) fits into pck2 (Figure 3B). An additional lowest-energy cluster (−8.22 kcal/mol) was identified in pck1b, although with ligand orientations head to tail with respect to the most populated and more significant pck1b cluster. Finally, although less populated, another cluster of A4 orientations was found in the central pck1a. For DHN2, the largest cluster (36 orientations, −9.44 kcal/mol) is located in pck3, followed by clusters placed in pck1b (16 orientations, −9.12 kcal/mol), and in pck1a (15 orientations, −10.05 kcal/mol; Figure 3C).

To verify if the above-described cavities are peculiar for the closed state of the protein, we repeated the blind docking simulations on the open conformational state of Hsp90. As anticipated, the homology model of human Hsp90 based on the *E.coli* HtpG open conformation[15] was built (Figure 5 in Supporting Information), and the MD simulation was performed using the same conditions previously applied for the closed state (see Supporting Information for details). Again, 500 conformations of the chaperone were collected, and the blind docking of the three inhibitors was performed on each conformation. Importantly, the most interesting clusters thus obtained still identified pck1a, pck1b, pck2, and pck3 (Figure 6 in Supporting Information). In particular,

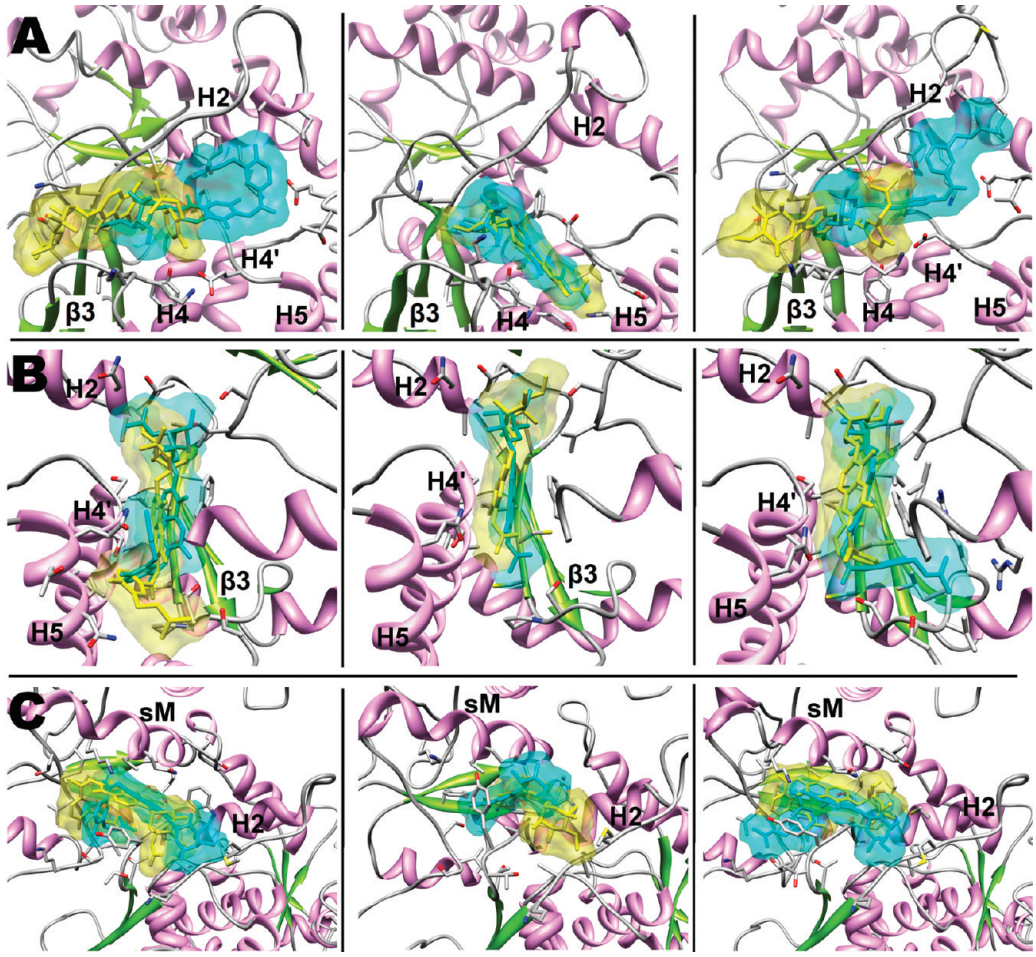

Figure 4. Binding modes of NB, A4, and DHN2 (column 1, 2, and 3) in pck1b (A), pck2 (B), and pck3 (C).

pck1a, pck1b, and pck3 were always populated by all three of the inhibitors. This behavior is consistent with the fact that in the open conformations these three pockets are wider than in the closed state, resulting in more populated clusters located in these cavities. Therefore, standing on these predictions, we can conclude that the blind docking results obtained for the open structures are qualitatively consistent with those already described for the closed structures and that the protein cavities where the coumarin inhibitors preferentially dock are similar in the two conformational states of Hsp90.

To sum up from the binding site identification step, four pockets were detected as putative binding sites for CT inhibitors. Three of these were found by all methods (pck1a, pck1b, and pck2), and an additional one emerged from blind docking (pck3).

As previously mentioned, these sites were further investigated with a subsequent focused docking step in order to infer the most likely binding site and to better characterize inhibitor binding modes. To this aim, independent focused docking experiments were carried out in the four predicted sites using two different docking programs (AutoDock and Glide).[31,32] This step is highly recommended because in a number of cases it was demonstrated that docking experiments restricted to predicted binding sites improved the results obtained from the blind docking procedure in terms of ligand binding poses and binding free energy estimations.[26,27] In addition, since docking scoring functions often fail to correctly estimate ligand binding free energies that correlate with experimental activities, the docking solutions were refined and rescored with the BEAR postdocking procedure developed in our lab,[33−36] which applies more accurate scoring functions for binding free energy estimation, such as molecular mechanics Poisson−Boltzmann surface area (MM-PBSA) and generalized Born surface area (MM-GBSA) (see Supporting Information for methodological details). Therefore, using BEAR, both AutoDock and Glide poses were refined with energy minimization of the corresponding Hsp90 complexes and then scored with MM-PBSA and -GBSA, generating two additional scores per pose. In the end, a consensus scoring strategy based on the rank-by-rank approach[37] was applied to rank and prioritize ligand poses in the cavities. The top 15 consensus results, for each cavity and ligand, based on AutoDock, MM-PBSA and -GBSA scores (hereafter named AD series), and Glide, MM-PBSA and -GBSA scores (Glide series) are reported in Table 1of the Supporting Information. In addition, the energy consensus was accompanied by a geometrical one. First, for each pocket, we searched for similar binding modes of a ligand between the AD and the Glide series, and second, since we used a set of congeneric inhibitors, we checked if the selected poses of NB, A4, and DHN2 were comparable. Based on these two criteria, the binding pose for each inhibitor was selected, and it is shown in Figure 4 and also in Figures 7 and 8 and highlighted in bold in Table 1 of the Supporting Information. Within the top 15 ranked solutions, a geometrical consensus was easily found for three of the four identified pockets (pck1b, pck2, and pck3), while in

the remaining pocket (pck1a), ligand poses were very different between both the AD and Glide series and among the three analogues, indicating a less specific binding mode of the inhibitors in this cavity.

In pck1b, while the A4 docked poses generated by AutoDock and Glide are well superimposed (Figure 4A, column 2 and also Figures 7A and 8A, column 2, in Supporting Information), NB and DHN2 poses are not (Figure 4A, columns 1 and 3). Despite this, a general scheme of orientation is observed with the noviose moiety exposed to the solvent and the benzamide group pointing toward the interior of the pocket. In particular, the sugar and the coumarin rings interact with Lys631, Lys632, Lys576, and Glu584 located onto H1 and loops connecting H1-β1 and H2-β3, while Ala629 and Tyr627 make hydrophobic contacts with the coumarin, benzamide, and isopentenyl chain. It is worth noting that MM-PBSA and -GBSA scores in the AD series are particularly favorable (see Table 1 in Supporting Information) when the hydroxyl group of the benzamide hydrogen bonds with Lys582 and Glu679 of loops H1-β1 and H4−H5. These binding modes are in agreement with structure−activity relationship (SAR) hypotheses, which show that a group with hydrogen-bond donor and acceptor capabilities on the aryl substituent increases inhibitory activity of CT-inhibitors.[38]

In pck2, the coumarin ring of the three inhibitors is deeply inserted into the channel formed by H4′ and β-strands and makes hydrophobic interactions with Phe507. The sugar moiety into the upper side of the pocket hydrogen bonds with the backbone of Thr607 and Ala608 located at the beginning of helix H2 and Thr495 of sM (Figure 4 B and also Figures 7B and 8B in Supporting Information).

In pck3, the selected poses are highly exposed to solvent, with a more external noviose moiety and the coumarin ring interacting with hydrophobic residues at the beginning of helix H2 (Tyr604 and Trp606) and the benzamide and isopentenyl chain anchored into the pocket above Val544 (Figure 4C and also Figures 7C and 8C in Supporting Information).

Comparing binding free energy values for each ligand in the three pockets, poses belonging to pck2 generally have better scores according to AutoDock, Glide, and MM-GBSA scoring functions. Values of pck1b and pck3, although lower than pck2, are comparable, except for better MM-PBSA scores in pck1b for the three inhibitors. Hence, going on geometrical and energetic criteria, our analysis suggests pck2 as the most likely CT binding site followed by pk1b and to a lesser extent pck3. Notably, the first two pockets, pck2 and pck1b, are lined by residues belonging to a segment of the dimerization region (YETALLSSGFSLED), which was proposed as contributing to the formation of the binding site.[4] Furthermore, both cavities have important structural motifs for chaperone activity. Pck2 contains a Cys residue that if S-nitrosylated affects the ATPase activity of Hsp90.[39] In this case, inhibitors interacting with this Cys residue could have similar effects on the chaperone function. On the other hand, pck1b is located between two segments on helices H1 and H2 relevant for the interaction between Hsp90 and the glucocorticoid receptor (GR), a well-known client protein of the chaperone.[40] The binding of inhibitors in pck1b could prevent the association between Hsp90 and GR, thus disrupting the activity of the chaperone.

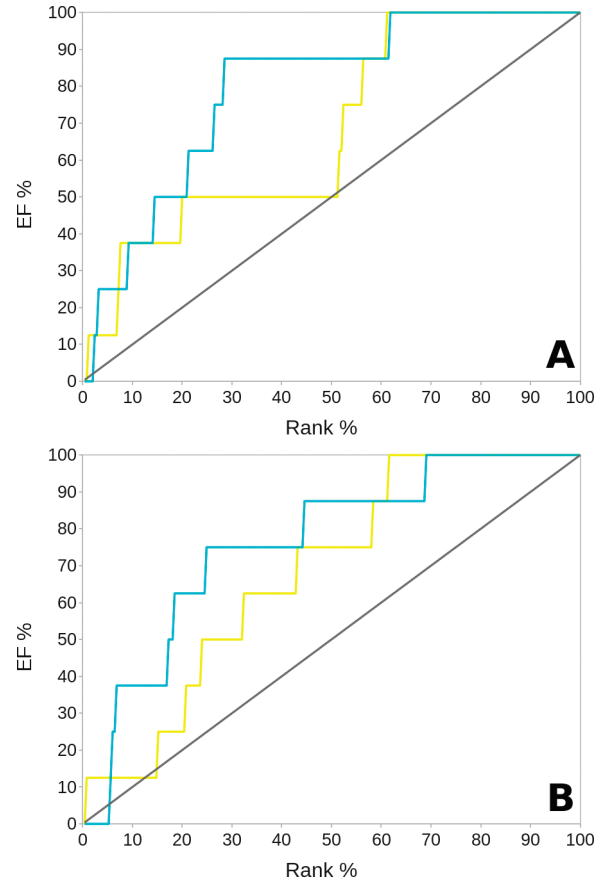

Figure 5. EFs obtained after docking and BEAR refinement and rescoring in pck1b (A) and pck2 (B). The yellow and cyan lines represent the EF curves of the AD and Glide series, respectively. Each curve was obtained from consensus scoring among AutoDock, MM-PBSA, and MM-GBSA (yellow) and Glide, MM-PBSA, and MM-GBSA (cyan). The gray line corresponds to a random selection.

Finally, in order to evaluate whether the identified pockets are able to enrich known ligands with respect to decoy molecules, an enrichment factor (EF) analysis in pck2 and pck1b was performed using the same approach put forward by Shoichet and Irwin[41] in their Directory of Useful Decoys (DUD). For this analysis we used a set of eight known inhibitors (NB, A4, and DHN2 complemented by five additional coumarin analogues selected among the most potent compounds developed so far[10,42−44] (Table 2 in Supporting Information) and 288 decoy molecules (36 decoys for each inhibitor) that resemble the physical properties of the ligands but are chemically and topologically distinct from them. Inhibitors and decoys were docked into pck1b and pck2 with the same parameters used for focused docking experiments and then refined and rescored using BEAR with identical settings (see Supporting Information for details). In these experiments, the higher the percentage of known ligands found at a given percentage of the ranked database, the better the enrichment performance of the virtual screen. The EF curves obtained from consensus scoring among AutoDock, MM-PBSA, and -GBSA and Glide, MM-PBSA, and -GBSA show that the known ligands rank significantly better than decoys in both pockets (Figure 5A and B), thus reinforcing the prediction of pck2 and pck1b as likely binding sites for the CT inhibitors. In particular, the two curves increase rapidly in the first 20% of the ranked data set, in which almost 50% of the known active ligands are found.

In conclusion, in the present study, we have obtained a three-dimensional structure of the full-length human Hsp90, which has not been experimentally determined yet, and we have employed major efforts toward exploring the challenging and hitherto unknown binding site located in the CT domain. By exploiting the conformational plasticity of the chaperone in two different states (closed and open) and applying many computational approaches for binding site identification, our simulations suggest that the most likely binding site is located in pck2 followed by pck1b.

These data provide a starting point for further experimental studies aimed at validating the binding poses identified in this work. It will prove interesting to see whether crystallographic analyses of Hsp90-CT inhibitor complexes confirm these results. Going on our results, we anticipate that the high conformational flexibility observed with MD simulations may pose a challenge toward the achievement of these structures and that inhibitor binding modes might show significant conformational dependencies. Likewise, mutagenesis studies of residues identified in our computational study may be useful to shed light on the more likely interaction site.

Undoubtedly, the characterization of the binding site in the C-terminal domain of human Hsp90 will have a strong impact on the rational design of new inhibitors acting with a novel mechanism and will provide a framework for future focused experiments increasing the likelihood of finding new effective anticancer drugs.

ACKNOWLEDGMENT

We thank A. Del Rio (University of Modena and Reggio Emilia) for a python script to perform cluster analysis, M.D. Parenti (University of Modena and Reggio Emilia) for building decoy molecules starting from the structures of known CT inhibitors, and F. Caporuscio (University of Modena and Reggio Emilia) for helpful discussions.

Supporting Information Available: Methodological details about homology model of full-length human Hsp90; molecular dynamics simulation of hHsp90; identification of the CT binding site; blind docking of three known CT inhibitors in sM-CT domains; focused docking and post-docking procedure. Several figures and two tables are also included.

This information is available free of charge via the Internet at http://pubs.acs.org/.

REFERENCES AND NOTES

(1) Pratt, W. B.; Toft, D. O. Steroid receptor interactions with heat shock protein and immunophilin chaperones. *Endocr. Rev.* **1997**, *18*, 306–360.

(2) Blagosklonny, M. V.; Toretsky, J.; Bohen, S.; Neckers, L. Mutant conformation of p53 translated in vitro or in vivo requires functional Hsp90. *Proc. Natl. Acad. Sci. U.S.A.* **1996**, *93*, 8379–8383.

(3) Söti, C.; Rácz, A.; Csermely, P. A nucleotide-dependent molecular switch controls ATP binding at the C-terminal domain of Hsp90. N-terminal nucleotide binding unmasks a C-terminal binding pocket. *J. Biol. Chem.* **2002**, *277*, 7066–7075.

(4) Marcu, M. G.; Chadli, A.; Bouhouche, I.; Catelli, M.; Neckers, L. M. The heat shock protein 90 antagonist novobiocin interacts with a previously unrecognized ATP-binding domain in the carboxyl terminus of the chaperone. *J. Biol. Chem.* **2000**, *275*, 37181–37186.

(5) Garnier, C.; Lafitte, D.; Tsvetkov, P. O.; Barbier, P.; Leclerc-Devin, J.; Millot, J.; Briand, C.; Makarov, A. A.; Catelli, M. G.; Peyrot, V. Binding of ATP to heat shock protein 90: evidence for an ATP-binding site in the C-terminal domain. *J. Biol. Chem.* **2002**, *277*, 12208–12214.

(6) Allan, R. K.; Mok, D.; Ward, B. K.; Ratajczak, T. Modulation of chaperone function and cochaperone interaction by novobiocin in the C-terminal domain of Hsp90: evidence that coumarin antibiotics disrupt Hsp90 dimerization. *J. Biol. Chem.* **2006**, *281*, 7161–7171.

(7) Chakraborty, A.; Koldobskiy, M. A.; Sixt, K. M.; Juluri, K. R.; Mustafa, A. K.; Snowman, A. M.; van Rossum, D. B.; Patterson, R. L.; Snyder, S. H. Hsp90 regulates cell survival via inositol hexakisphosphate kinase-2. *Proc. Natl. Acad. Sci. U.S.A.* **2008**, *105*, 1134–1139.

(8) Marcu, M. G.; Schulte, T. W.; Neckers, L. Novobiocin and related coumarins and depletion of heat shock protein 90-dependent signaling proteins. *J. Natl. Cancer Inst.* **2000**, *92*, 242–248.

(9) Yu, X. M.; Shen, G.; Neckers, L.; Blake, H.; Holzbeierlein, J.; Cronk, B.; Blagg, B. S. J. Hsp90 inhibitors identified from a library of novobiocin analogues. *J. Am. Chem. Soc.* **2005**, *127*, 12778–12779.

(10) Burlison, J. A.; Neckers, L.; Smith, A. B.; Maxwell, A.; Blagg, B. S. J. Novobiocin: redesigning a DNA Gyrase inhibitor for selective inhibition of Hsp90. *J. Am. Chem. Soc.* **2006**, *128*, 15529–15536.

(11) Burlison, J. A.; Blagg, B. S. J. Synthesis and evaluation of coumermycin A1 analogues that inhibit the Hsp90 protein folding machinery. *Org. Lett.* **2006**, *8*, 4855–4858.

(12) Lin, J.; Perryman, A. L.; Schames, J. R.; McCammon, J. A. Computational drug design accommodating receptor flexibility: the relaxed complex scheme. *J. Am. Chem. Soc.* **2002**, *124*, 5632–5633.

(13) Lin, J.; Perryman, A. L.; Schames, J. R.; McCammon, J. A. The relaxed complex method: accommodating receptor flexibility for drug design with an improved scoring scheme. *Biopolymers* **2003**, *68*, 47–62.

(14) Mayer, M. P.; Prodromou, C.; Frydman, J. The Hsp90 mosaic: a picture emerges. *Nat. Struct. Mol. Biol.* **2009**, *16*, 2–6.

(15) Shiau, A. K.; Harris, S. F.; Southworth, D. R.; Agard, D. A. Structural analysis of E. coli Hsp90 reveals dramatic nucleotide-dependent conformational rearrangements. *Cell* **2006**, *127*, 329–340.

(16) Southworth, D. R.; Agard, D. A. Species-dependent ensembles of conserved conformational states define the Hsp90 chaperone ATPase cycle. *Mol. Cell* **2008**, *32*, 631–640.

(17) Ali, M. M. U.; Roe, S. M.; Vaughan, C. K.; Meyer, P.; Panaretou, B.; Piper, P. W.; Prodromou, C.; Pearl, L. H. Crystal structure of an Hsp90-nucleotide-p23/sba1 closed chaperone complex. *Nature* **2006**, *440*, 1013–1017.

(18) Sippl, M. J. Recognition of errors in three-dimensional structures of proteins. *Proteins* **1993**, *17*, 355–362.

(19) Eramian, D.; Shen, M.; Devos, D.; Melo, F.; Sali, A.; Marti-Renom, M. A. A composite score for predicting errors in protein structure models. *Protein Sci.* **2006**, *15*, 1653–1666.

(20) Laskowski, R.; MacArthur, M.; Moss, D.; Thornton, J. Procheck: a program to check the stereochemical quality of protein structures. *J. Appl. Crystallogr.* **1993**, *26*, 283–291.

(21) Bron, P.; Giudice, E.; Rolland, J.; Buey, R. M.; Barbier, P.; Díaz, J. F.; Peyrot, V.; Thomas, D.; Garnier, C. Apo-Hsp90 coexists in two open conformational states in solution. *Biol. Cell* **2008**, *100*, 413–425.

(22) Dollins, D. E.; Warren, J. J.; Immormino, R. M.; Gewirth, D. T. Structures of Grp94-nucleotide complexes reveal mechanistic differences between the Hsp90 chaperones. *Mol. Cell* **2007**, *28*, 41–56.

(23) Krukenberg, K. A.; Förster, F.; Rice, L. M.; Sali, A.; Agard, D. A. Multiple conformations of E. coli Hsp90 in solution: insights into the conformational dynamics of Hsp90. *Structure* **2008**, *16*, 755–765.

(24) Harris, R.; Olson, A. J.; Goodsell, D. S. Automated prediction of ligand-binding sites in proteins. *Proteins* **2008**, *70*, 1506–1517.

(25) Halgren, T. A. Identifying and characterizing binding sites and assessing druggability. *J. Chem. Inf. Model.* **2009**, *49*, 377–389.

(26) Hetényi, C.; van der Spoel, D. Efficient docking of peptides to proteins without prior knowledge of the binding site. *Protein Sci.* **2002**, *11*, 1729–1737.

(27) Hetényi, C.; van der Spoel, D. Blind docking of drug-sized compounds to proteins with up to a thousand residues. *FEBS Lett.* **2006**, *580*, 1447–1450.

(28) Iorga, B.; Herlem, D.; Barré, E.; Guillou, C. Acetylcholine nicotinic receptors: finding the putative binding site of allosteric modulators using the "blind docking" approach. *J. Mol. Model.* **2006**, *12*, 366–372.

(29) Vasko, R. C.; Rodriguez, R. A.; Cunningham, C. N.; Ardi, V. C.; Agard, D. A.; McAlpine, S. R. Mechanistic studies of sansalvamide A-amide: an allosteric modulator of Hsp90. *ACS Med. Chem. Lett.* **2010**, *1*, 4–8.

(30) Sgobba, M.; Degliesposti, G.; Ferrari, A. M.; Rastelli, G. Structural models and binding site prediction of the C-terminal domain of human Hsp90: a new target for anticancer drugs. *Chem. Biol. Drug Des.* **2008**, *71*, 420–433.

(31) Huey, R.; Morris, G. M.; Olson, A. J.; Goodsell, D. S. A semiempirical free energy force field with charge-based desolvation. *J. Comput. Chem.* **2007**, *28*, 1145–1152.

(32) Friesner, R. A.; Banks, J. L.; Murphy, R. B.; Halgren, T. A.; Klicic, J. J.; Mainz, D. T.; Repasky, M. P.; Knoll, E. H.; Shelley, M.; Perry, J. K.; Shaw, D. E.; Francis, P.; Shenkin, P. S. Glide: a new approach for rapid, accurate docking and scoring. 1. method and assessment of docking accuracy. *J. Med. Chem.* **2004**, *47*, 1739–1749.

(33) Ferrari, A. M.; Degliesposti, G.; Sgobba, M.; Rastelli, G. Validation of an automated procedure for the prediction of relative free energies of binding on a set of aldose reductase inhibitors. *Bioorg. Med. Chem.* **2007**, *15*, 7865–7877.

(34) Rastelli, G.; Degliesposti, G.; Del Rio, A.; Sgobba, M. Binding estimation after refinement, a new automated procedure for the refinement and rescoring of docked ligands in virtual screening. *Chem. Biol. Drug Des.* **2009**, *73*, 283–286.

(35) Degliesposti, G.; Kasam, V.; Da Costa, A.; Kang, H.; Kim, N.; Kim, D.; Breton, V.; Kim, D.; Rastelli, G. Design and discovery of plasmepsin II inhibitors using an automated workflow on large-scale grids. *ChemMedChem* **2009**, *4*, 1164–1173.

(36) Rastelli, G.; Del Rio, A.; Degliesposti, G.; Sgobba, M. Fast and accurate predictions of binding free energies using MM-PBSA and MM-GBSA. *J. Comput. Chem.* **2010**, *31*, 797–810.

(37) Verdonk, M. L.; Berdini, V.; Hartshorn, M. J.; Mooij, W. T. M.; Murray, C. W.; Taylor, R. D.; Watson, P. Virtual screening using protein-ligand docking: avoiding artificial enrichment. *J. Chem. Inf. Comput. Sci.* **2004**, *44*, 793–806.

(38) Donnelly, A.; Blagg, B. S. J. Novobiocin and additional inhibitors of the Hsp90 C-terminal nucleotide-binding pocket. *Curr. Med. Chem.* **2008**, *15*, 2702–2717.

(39) Retzlaff, M.; Stahl, M.; Eberl, H. C.; Lagleder, S.; Beck, J.; Kessler, H.; Buchner, J. Hsp90 is regulated by a switch point in the C-terminal domain. *EMBO Rep.* **2009**, *10*, 1147–1153.

(40) Fang, L.; Ricketson, D.; Getubig, L.; Darimont, B. Unliganded and hormone-bound glucocorticoid receptors interact with distinct hydrophobic sites in the Hsp90 C-terminal domain. *Proc. Natl. Acad. Sci. U.S.A.* **2006**, *103*, 18487–18492.

(41) Huang, N.; Shoichet, B. K.; Irwin, J. J. Benchmarking sets for molecular docking. *J. Med. Chem.* **2006**, *49*, 6789–6801.

(42) Burlison, J. A.; Avila, C.; Vielhauer, G.; Lubbers, D. J.; Holzbeierlein, J.; Blagg, B. S. J. Development of novobiocin analogues that manifest anti-proliferative activity against several cancer cell lines. *J. Org. Chem.* **2008**, *73*, 2130–2137.

(43) Donnelly, A. C.; Mays, J. R.; Burlison, J. A.; Nelson, J. T.; Vielhauer, G.; Holzbeierlein, J.; Blagg, B. S. J. The design, synthesis, and evaluation of coumarin ring derivatives of the novobiocin scaffold that exhibit antiproliferative activity. *J. Org. Chem.* **2008**, *73*, 8901–8920.

(44) Shelton, S. N.; Shawgo, M. E.; Matthews, S. B.; Lu, Y.; Donnelly, A. C.; Szabla, K.; Tanol, M.; Vielhauer, G. A.; Rajewski, R. A.; Matts, R. L.; Blagg, B. S. J.; Robertson, J. D. KU135, a novel novobiocin-derived C-terminal inhibitor of the 90-kDa heat shock protein, exerts potent antiproliferative effects in human leukemic cells. *Mol. Pharmacol.* **2009**, *76*, 1314–1322.

CI1001857